# Porous Fe₂O₃ nanorods anchored on nitrogen-doped graphenes and ultrathin Al₂O₃ coating by atomic layer deposition for long-lived lithium ion battery anode

*Tao Hu [a,b], Ming Xie [c], Jing Zhong [d], Hong-tao Sun [b], Xiang Sun [b], Spencer Scott [b], Steven M. George [c], Chang-sheng Liu [a], Jie Lian [b,*]*

[a] *Key Laboratory for Anisotropy and Texture of Materials of Ministry of Education, Northeastern University, Shenyang, Liaoning 110004, China*
[b] *Department of Mechanical, Aerospace & Nuclear Engineering, Rensselaer Polytechnic Institute, Troy, NY 12180, USA*
[c] *Department of Chemistry and Biochemistry and Department of Mechanical Engineering, University of Colorado, Boulder, CO 80309, USA*
[d] *School of Civil Engineering, Harbin Institute of Technology, Harbin, Heilongjiang 150090, China*

ARTICLE INFO

ABSTRACT

Porous iron oxide ($Fe_2O_3$) nanorods anchored on nitrogen-doped graphene sheets (NGr) were synthesized by a one-step hydrothermal route. After a simple microwave treatment, the iron oxide and graphene composite (NGr-I-M) exhibits excellent electrochemical performances as an anode for lithium ion battery (LIB). A high reversible capacity of 1016 mAh $g^{-1}$ can be reached at 0.1 A $g^{-1}$. When NGr-I-M electrode was further coated by 2 ALD cycles of ultrathin $Al_2O_3$ film, the first cycle Coulombic efficiency (CE), rate performance and cycling stability of the coated electrode can be greatly improved. A stable capacity of 508 mAh $g^{-1}$ can be achieved at 2 A $g^{-1}$ for 200 cycles, and an impressive capacity of 249 mAh $g^{-1}$ at 20 A $g^{-1}$ can be maintained without capacity fading for 2000 cycles. The excellent electrochemical performance can be attributed to the synergy of porous iron oxide structures, nitrogen-doped graphene framework, and ultrathin $Al_2O_3$ film coating. These results highlight the importance of a rational design of electrode materials improving ionic and electron transports, and potential of using ALD ultrathin coatings to mitigate capacity fading for ultrafast and long-life battery electrodes.

## 1. Introduction

Rechargeable lithium ion batteries (LIBs) have been extensively utilized as secondary energy storage devices due to the increasing demands for portable electronic devices, and electrical vehicles [1–3]. However, the current graphite anode displays a relatively-low theoretical specific capacity (372 mAh $g^{-1}$) and poor rate capacity [4–6]. Therefore, it is essential to develop next generation electrode materials with high energy density, prolonged lifetime, and low costs. Although Li metal has a high theoretical capacity (3860 mAh $g^{-1}$) as anode for LIBs, two major drawbacks: (1)

continuous decomposition of the electrolyte, and (2) acceleration of dendritic growth and non-uniform morphology of the Li surface, can seriously affect the performance, cycle life, and safety of LIBs [7,8]. Transition metal oxides (MO) such as SnO$_2$ [9], CoO/Co$_3$O$_4$ [10,11], MnO$_2$ [12], Fe$_2$O$_3$/Fe$_3$O$_4$ [13,14], V$_2$O$_5$ [15], NiO [16], CuO [17] with higher theoretical capacities (>600 mAh g$^{-1}$) have been extensively investigated as anode materials for LIBs. Among them, iron-based MOs including Fe$_2$O$_3$, Fe$_3$O$_4$, and FeOOH are considered as the most promising candidates owing to their high theoretical capacity, low cost, and abundance [13,14,18], and therefore, have great potentials as alternative anodes for LIBs.

However, electrochemical applications of metal oxides are hindered by their inherently poor electrical conductivity and capacity fading arising from the large volume change that occurs upon Li$^+$ insertion and extraction [13,14,19–25]. Therefore, a variety of nanostructures including uniform nanotubes [13], nanowires [19], nanodiscs [20], nanorods [21,22] and other hierarchical nanostructures [23–25], were developed to provide shortened ionic and electronic transport paths, and avoid the pulverization of the active electrode materials. On the other hand, high-capacity metal oxides anchored with conductive carbonaceous materials have been extensively studied [9,10,12,14,23,26]. For instance, chemically-modified graphene compounds, e.g., nitrogen-doped graphene (NGr), has attracted attention due to their superior specific capacity under high charge rates. This was ascribed to the increased disorder on the surface, enhanced hydrophobicity, better electrode-electrolyte wettability, and improved electrochemical activity owing to the substitution of nitrogen atoms [27,28]. Moreover, the composite of Fe$_2$O$_3$ nanoparticles and NGr displayed good electrochemical performance due to the synergistic effect between small Fe$_2$O$_3$ particles and good electronic conductivity graphene sheets [29].

Here, we report a rational design of electrode materials by integrating porous MOs, nitrogen-doped graphene and ultra-thin coating by atomic layer deposition (ALD) to achieve excellent electrochemical performance for LIB anode applications. Particularly, a simple and one-step hydrothermal route was developed to synthesize porous iron oxide nanorods anchored on nitrogen-doped graphene sheets. Iron oxide nanorods were obtained from the reaction between FeSO$_4$ and OH$^-$ from alkaline urea. Importantly, urea gradually releases NH$_3$ that continually reacts with the oxygen functional groups of graphene oxide (GO), resulting in doping of nitrogen into the graphene structure [30]. After a subsequent hydrothermal process, porous iron oxide nanorods with a diameter of 20–30 nm, and length of 70–80 nm, were grown on the nitrogen-doped graphene sheets forming the composite of iron oxide and nitrogen-doped graphene (NGr-I). Then, a rapid and convenient microwave treatment was used to remove the remaining oxide functional groups from graphene sheets to obtain the NGr-I-M.

In order to further improve the lifetime of composite electrode, ultrathin Al$_2$O$_3$ layer was directly deposited on the composite electrode by ALD. Al$_2$O$_3$ ALD can serve artificial SEI film to protect the surface of the active electrode powders, maintain an inter-particle electronic pathway, and also act as a binding agent to hold active materials together to avoid pulveriza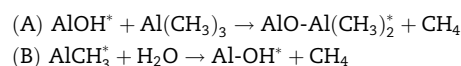tion due to large volume change [31,32]. The ultrathin Al$_2$O$_3$ coating by 2 ALD cycles greatly improve the first cycle Coulombic efficiency (CE), and enhance the cyclic stability upon prolong cycles and at high rates. The coated NGr-I-M composite electrode exhibits a high capacity of 508 mAh g$^{-1}$ at 2 A g$^{-1}$ for 200 cycles, and an impressive capacity of 249 mAh g$^{-1}$ can be preserved without any capacity fading after 2000 cycles at 20 A g$^{-1}$.

## 2. Experimental section

### 2.1. Materials preparation

GO was synthesized from natural graphite flake using a modified Hummers method, the details of which are described in a previous work [26]. NGr-I was synthesized by a simultaneous hydrothermal synthesis and assembly procedure. In a typical procedure, 30 ml 2 mg ml$^{-1}$ GO solution was mixed with 5.4 g urea by sonication for 30 min. 3 mmol FeSO$_4$·7H$_2$O was introduced followed by a 30 min ultra-sonication. The mixture was transferred to a polytetrafluoroethylene (Telfon)-lined autoclave and hydrothermally treated at 160 °C for 15 h. Finally, the NGr-I was obtained after washing several times, followed by vacuum drying overnight. NGr-I-M was prepared by microwave treating NGr-I for 2 min using a household microwave oven (700 W, Galanz) to eliminate the oxygen functional groups on the surface of graphene sheets.

Al$_2$O$_3$ ALD was deposited using trimethylaluminium (TMA) and H$_2$O as the precursors on the fabricated NGr-I and NGr-I-M electrodes based on following two reactions [33–35].

(A) AlOH$^*$ + Al(CH$_3$)$_3$ → AlO-Al(CH$_3$)$_2^*$ + CH$_4$
(B) AlCH$_3^*$ + H$_2$O → Al-OH$^*$ + CH$_4$

where the asterisks indicate the surface species. The combination of the A and B reactions constitutes one Al$_2$O$_3$ ALD cycle. HPLC (high performance liquid chromatography) grade H$_2$O and 97% TMA were obtained from Sigma–Aldrich. The Al$_2$O$_3$ ALD reaction sequence was: (i) dose TMA to 1.0 Torr for 120 s; (ii) evacuate reaction products and excess TMA; (iii) dose N$_2$ to 20.0 Torr for 60 s and then evacuate N$_2$ (repeat 5 times); (iv) dose H$_2$O to 1.0 Torr for 120 s, (v) evacuate reaction products and excess H$_2$O; and (vi) dose N$_2$ to 20.0 Torr for 60 s and then evacuate N$_2$ (repeat 5 times). This sequence constitutes one AB cycle of Al$_2$O$_3$ ALD. The Al$_2$O$_3$ ALD was performed for 2 cycles at 180 °C.

### 2.2. Structural and electrochemical characterization

The structural, morphological, and microstructural properties of the graphene and iron oxide nanocomposites were characterized using a variety of techniques. X-ray diffraction (XRD) measurements were tested using a PANanalytical X-ray diffraction system with Cu radiation at 45 kV, 40 mA. Scanning electron microscopy (SEM) images were acquired by a Carl Zeiss Ultra 1540 Dual Beam FIB/SEM System. Transmission electron microscopy (TEM) images were obtained using a JEOL JEM-2010 instrument with an operating voltage of 200 kV. Thermogravimetric analysis (TGA) measurements were performed in air from 30 to 800 °C at a heating rate of 10 °C/

min in a TA Instrument TGA-Q50. The X-ray photoelectron spectrum was recorded on a PHI 5000 Versa Probe system.

### 2.3. Electrochemical measurements

Electrochemical performance of the composite electrode was investigated using a coin cell configuration with a lithium metal foil as the counter electrode. The working electrode was fabricated by a slurry coating procedure, in which active materials, carbon black and PVDF were mixed at a weight ratio of 80:10:10 in N-methylpyrrolidinone (NMP), then coated on the Cu foil and dried under 80 °C overnight in vacuum.

2032 coin cells were assembled in an argon-filled glove box with the electrolyte consisting of 1 M $LiPF_6$ dissolved in the solution with 1:1 ethylene carbonate and diethyl carbonate by volume (Novolyte Technologies), and used a Celgard separator 2340. The electrochemical behaviors of the electrodes were characterized using an Arbin BT 2000 testing station, operated between 0.01 and 3.0 V vs. $Li^+/Li$. The cyclic voltammetry (CV) and Nyquist plots were analyzed using a potentiostat VersaSTAT 4 (Princeton Applied Research). All the electrochemical measurements were carried out at room temperature. All capacities are calculated on the basis of the total mass of the hybrid materials in this work and the mass loadings were around 1.6 mg cm$^{-2}$.
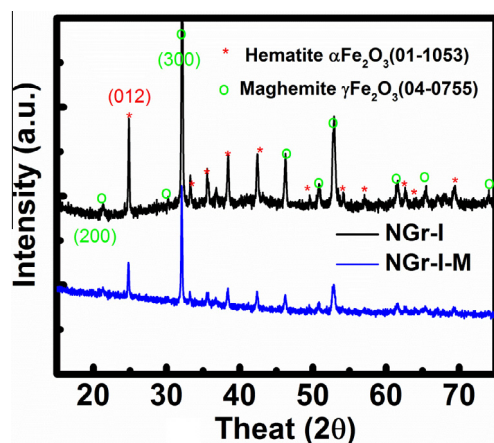


**Fig. 1 – XRD patterns of the NGr-I and NGr-I-M composites. (A colour version of this figure can be viewed online.)**

## 3. Results and discussions

### 3.1. Materials characterizations

As shown in the Fig. 1, both hematite ($\alpha$) and maghemite ($\gamma$) $Fe_2O_3$ crystal structures coexist in the composites. The peaks located at $2\theta = 21°$ and 25° correspond to the (200) and (012) lattice planes of the $\alpha$ and $\gamma$ $Fe_2O_3$ (JCPDS 01-1053 and 04-0755), respectively. Moreover, the microwave oven treatment does not change the crystal structure of the metal oxides, which is supported by the fact that NGr-I-M peaks were found overlapped with the same peaks of NGr-I.

TEM images (Fig. 2) show the morphology of the hybrid composite of the iron oxide nanorods on graphene sheets. The anchoring of iron oxide nanorods on graphene sheets was clearly revealed by the TEM image (as shown in Fig. 2a), showing cylindrical and short $Fe_2O_3$ nanorods with length of $\sim$70 nm and diameter of 20–30 nm distributed between the layers of graphene. The integration of $Fe_2O_3$ nanorods with graphene sheets can facilitate electron transfer during charge/discharge. A high resolution TEM image (Fig. 2b) clearly shows the porous feature of the iron oxide nanorods with the pore size about 8–9 nm. The $NH_3$ released from urea promotes the formation of pores on the surface of iron oxides during a long hydrothermal process (15 h). The lattice fringe spacing was determined to be 0.368 and 0.418 nm in the high-resolution TEM (HRTEM) image (see Fig. 2c), corresponding to the (012) and (200) lattice planes of $\alpha$ and $\gamma$ $Fe_2O_3$, respectively, consistent with the XRD results.

TGA analysis further determined the weight ratio of graphene and iron oxide composites. As shown in TGA results of the NGr-I and NGr-I-M (see Fig. 3), the 1% weight loss near 250 °C can be attributed to adsorbed water molecules. The weight loss from 300 to 550 °C may be attributed to the consumption of graphene, resulting in 72 wt% and 73 wt% loadings of $Fe_2O_3$ in the NGr-I and NGr-I-M, respectively [22]. It is worth noting that the 1% weight gap between NGr-I and NGr-I-M may be attributed to the removal of residual oxygen groups by microwave treatment.

During the synthesis processes, 1.2% atomic ratio of nitrogen was doped into the graphene composites (see Fig. 4a) [36]. Additionally, as shown in the XPS spectrum (Fig. 4b), the peaks at 711 and 724 eV in the Fe 2p spectrum may be attributed to the Fe 2p3/2 and Fe 2p1/2, respectively [19,24]. Two peaks at 530.1 and 532.1 eV can be observed in the O 1s
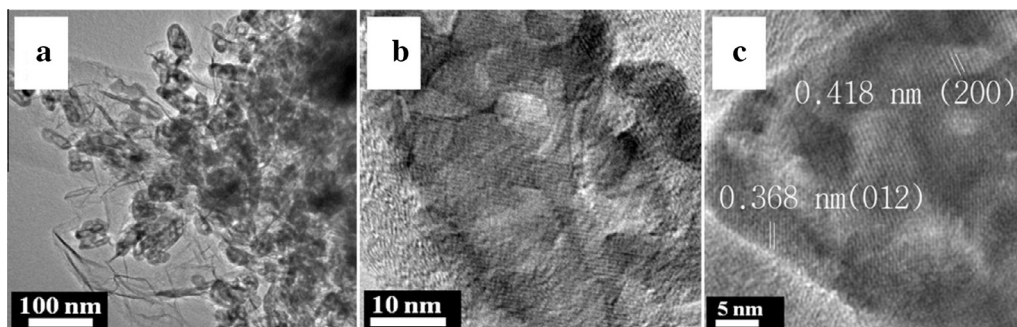


**Fig. 2 – Morphology and microstructure of the composite electrodes: (a–c) TEM images of NGr-I nanostructures.**
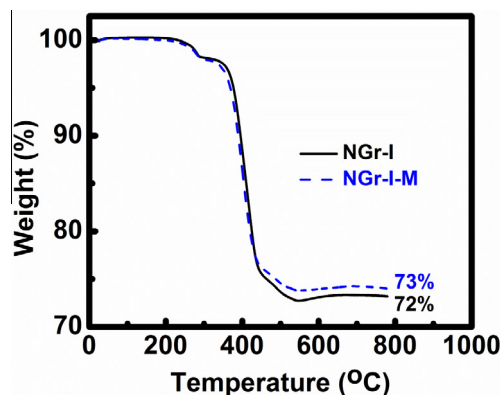
**Fig. 3 – TGA curves of NGr-I and NGr-I-M. (A colour version of this figure can be viewed online.)**

spectrum (see Fig. 4c). The former can be attributed to the presence of $O^{2-}$, and the latter one can be assigned to C=O [24]. The absence of peaks at 531 and 533 eV, which correspond to $OH^-$ and $H_2O$ respectively [24], indicates no existence of FeOOH in the composites, consistent with XRD.

As displayed in the Fig. 4d, four components of C1s bonds including C=C, C–OH, C=O, and O–C=O can be observed in the C1s spectra of the NGr-I-M with peaks located at 284.6, 285.8, 288.03, and 289.8 eV, respectively. However, peaks of C=C and O–C=O are the most prominent, indicating the presence of a graphene structure with well bonded iron oxides for the NGr-I-M composite [37].

### 3.2. Electrochemical characterizations

The electrochemical properties of the graphene–$Fe_2O_3$ nanorod composites as anode materials for LIBs were examined by cyclic voltammogram (CV). CV of the NGr-I-M electrode at a scan rate of 0.5 mV s$^{-1}$ for first five cycles is shown in Fig. 5a. In the first cycle, cathode peaks at 1.44, 0.8, and

0.35 V may be attributed to the stepwise reduction of $Fe^{3+}$ to $Fe^{2+}$ and Fe and the formation of solid electrolyte interface (SEI) film, respectively [14,38]. In the anodic process, two peaks at 1.62 and 1.83 V can be ascribed to the oxidation of $Fe^0$ back to $Fe^{3+}$ [14,24]. In the subsequent cycles, the peaks at lower potentials disappear, revealing that the formation of the SEI layer primarily occurred during the first cycle; while the other voltage peaks shift to higher potentials. The oxidation peaks, remaining nearly unchanged, indicate a good reversibility of the $Fe^0$ to $Fe^{3+}$ reaction [14].

Fig. 5b shows the rate capability of the NGr-I and NGr-I-M composite electrodes, at different current densities from 0.1 to 0.3, 0.5, 1, 2, and 3 A g$^{-1}$. The hybrid NGr-I-M electrode exhibits a much higher capacity upon microwave treatment. A high reversible capacity of 1016 mAh g$^{-1}$ can be obtained at 0.1 A g$^{-1}$ for NGr-I-M. Moreover, at high current densities of 2 and 3 A g$^{-1}$, higher discharge capacities are achieved for the NGr-I-M electrode (651 and 522 mAh g$^{-1}$) than the NGr-I electrode (437 and 226 mAh g$^{-1}$), respectively. To our best knowledge, these results are superior to previous iron oxides results reported in the literatures [13,14,20–22,25,38]. These excellent capacities might be a result of microwave treatment improving the conductivity of hybrid anodes by removing the excess oxygen functional groups of graphene sheets. The assumption can be confirmed by an electrochemical impedance spectroscopy (EIS) measurement. The Nyquist plots in Fig. 5c reveal that the NGr-I-M electrode has a lower charge transfer resistance ($R_{CT}$ = 165.66 Ω) than that of the NGr-I electrode, and a lower $Z_w$ compared to the NGr-I electrode, due to the faster diffusion of Li$^+$ [27]. The charge and discharge plateaus of the NGr-I-M electrode can be seen at all current densities from 0.3 to 3 A g$^{-1}$ (see Fig. 5d). The initial discharge and charge capacities of the NGr-I-M electrode are 1701 and 1100 mAh g$^{-1}$ at 0.1 A g$^{-1}$, respectively. The Coulombic efficiency was around 65% which can be attributed to the possible irreversible processes such as electrolyte decomposition and the formation of SEI [5,14,22]. When the current densities
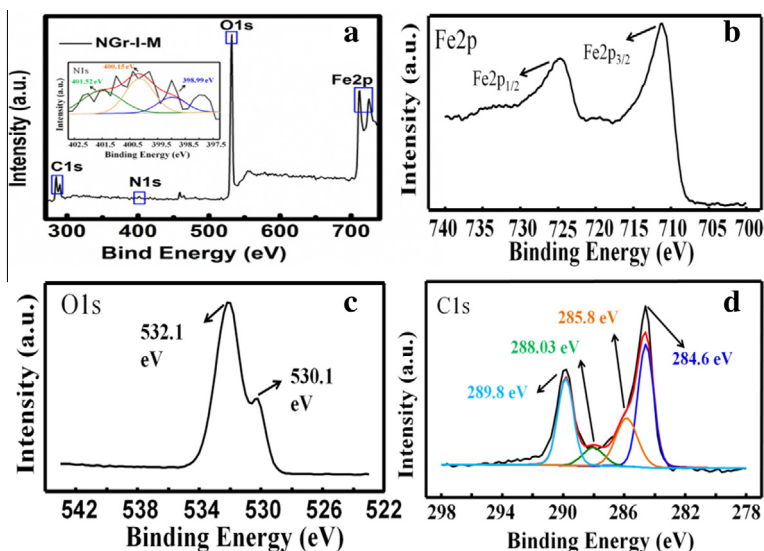


**Fig. 4 – (a) XPS spectra of the NGr-I-M composite (inset pattern is N1s spectra) and high-resolution Fe2p (b), O1s (c), and C1s (d) spectra. (A colour version of this figure can be viewed online.)**
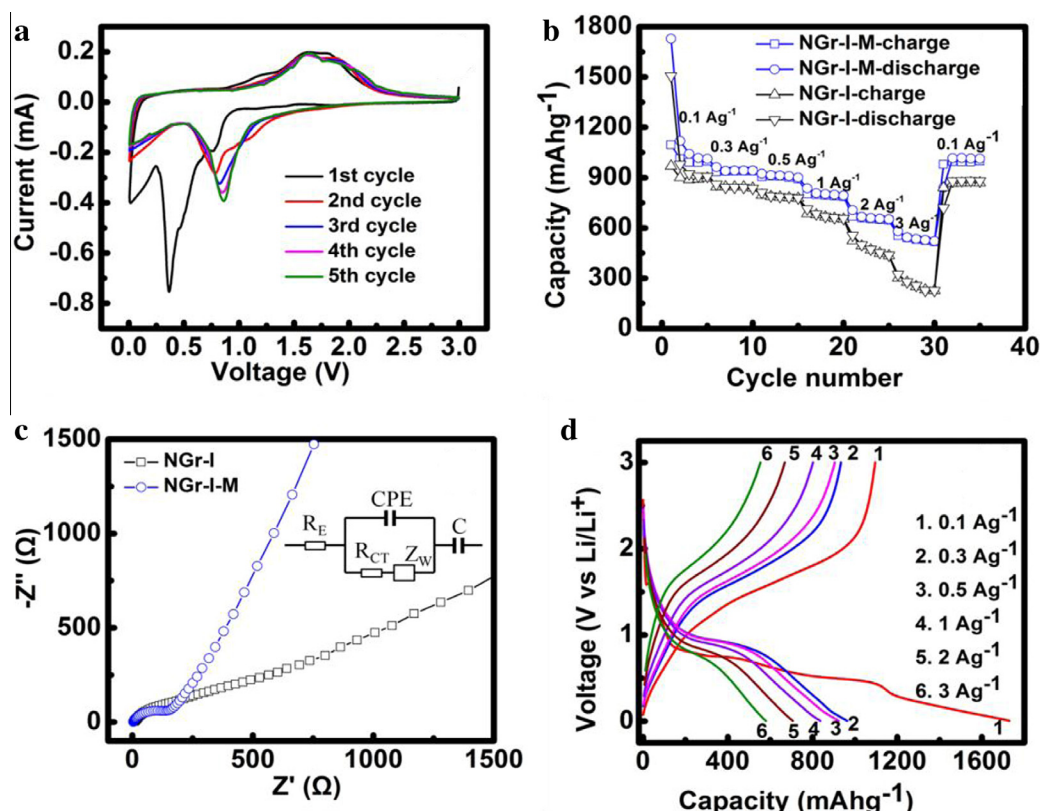
**Fig. 5 – Electrochemical performance of the graphene and iron oxide composite electrodes. (a) CVs curves of the NGr-I-M electrode at a scan rate of 0.5 mV s$^{-1}$ for five cycles. (b) Rate capacities of the NGr-I and NGr-I-M electrodes at various current densities. (c) Nyquist plots of the NGr-I and NGr-I-M electrodes at a discharged potential of 0.1 V (vs. Li/Li$^+$) from 100 kHz to 10 mHz (inset, modeled equivalent circuit of EIS). (d) Representative discharge-charge curves of the NGr-I-M anode at various current rates for the first cycle. (A colour version of this figure can be viewed online.)**

increased to higher rates, the Coulombic efficiency have improved to 96.9%, 98.1%, 95.9%, 94.8%, and 95.5% at 0.3, 0.5, 1, 2, and 3 A g$^{-1}$, respectively.

However, capacity decay still occurs for both NGr-I-M and NGr-I electrodes. By depositing ultrathin Al$_2$O$_3$ film (~5 Å) on the electrode via ALD, the initial cycling Coulombic efficiency can be significantly improved, and the capacity fading at prolong cycles can be greatly mitigated. Particularly, for the NGr-I-M-2ALD, the Coulombic efficiency of the first cycle is 89%, much higher than uncoated electrodes NGr-I-M (65%). Moreover, for both ALD coating electrodes, the Coulombic efficiency steadily reaches around 99% after three cycles under 2 A g$^{-1}$, which can be attributed to that the active materials from electrodes are able to maintain their structural integrity and their electrical contact with 2 cycles Al$_2$O$_3$ ALD coating.

The ALD-Al$_2$O$_3$ coated electrodes also display excellent rate performance and capacity retention capabilities at long cycles. As shown in the Fig. 6a, the reversible discharge capacity of the NG-I-2ALD electrode (coated with 2 cycles Al$_2$O$_3$ film) can sustain 428 mAh g$^{-1}$ after 200 cycles under a high current density of 2 A g$^{-1}$, which is around 4.7 times higher than that of the NG-I anode (91 mAh g$^{-1}$) without ALD coating. Furthermore, a reversible discharge capacity as high as 508 mAh g$^{-1}$ can be obtained for the NG-I-M-2ALD (2 cycles

Al$_2$O$_3$ film) after 200 cycles under 2 A g$^{-1}$. The much lower capacity from uncoated samples may be attributed to electrode pulverization during cycling, resulting in a loss of electrical contact between a portion of active material and current collector. Furthermore, 2 cycles Al$_2$O$_3$ coating is thin enough, allowing lithium ion diffusion even at high rates.

The enhanced rate performance and cyclic stability of the ALD coated composite electrode by ultrathin Al$_2$O$_3$ films are consistent with previous studies [31,32], in which the stability of LIB electrodes can be significantly improved by adding ultrathin (<1 nm) conformal Al$_2$O$_3$ coatings to as-fabricated electrodes directly. It is believed that an Al$_2$O$_3$ ALD layer can serve as artificial SEI and protect the surface of the active materials in electrodes while still enabling electrical conductivity and structural integrity during the charge-discharge cycle [31,32]. This effect may be further enhanced in materials suffering severe pulverization during cycling.

The cycle retention and capacity performance of the NGr-I-M-2ALD anode were further evaluated at 20 A g$^{-1}$ for 2000 cycles. As shown in the Fig. 6b, a reversible capacity of 249 mAh g$^{-1}$ was obtained with nearly 100% Coulombic efficiency. This enhanced electrochemical performance can be attributed to a combination of: (1) porous iron oxides nanostructures, which may increase the interface between the active materials and the electrolyte; (2) flexible graphene
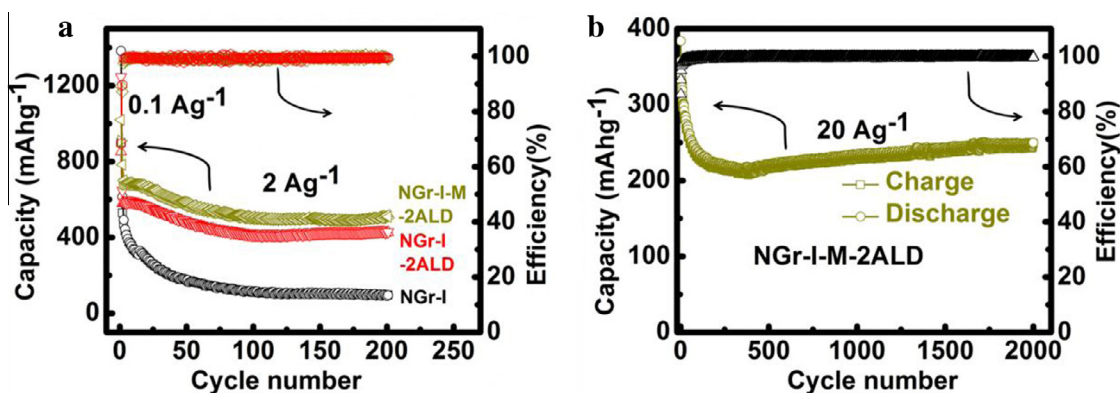
**Fig. 6 – Cycle performance of the composite electrodes: (a) the NGr-I, NGr-I-2ALD, and NGr-I-M-2ALD electrodes when performing full discharge-charge at 2 A g$^{-1}$ for 200 cycles. (b) Capacity performance of the NGr-I-M-2ALD at an extremely high current rate of 20 A g$^{-1}$ for 2000 cycles. (A colour version of this figure can be viewed online.)**

sheets, which can not only buffer the volume change of $Fe_2O_3$ nanorods during Li$^+$ insertion/extraction, but also enhance the conductivity of electrodes; (3) N doping, which helps further improve the conductivity of graphene sheets and capacity; and (4) the ultrathin $Al_2O_3$ film coating on the electrode, which can help maintain electrical contact between the active electrode materials and current collector, therefore improving the long cycle retention under the increased current of 20 A g$^{-1}$.

## 4.    Conclusions

In summary, a facile and one-step synthesis route was developed to synthesize a nitrogen-doped graphene and $Fe_2O_3$ nanorod composite, where porous $Fe_2O_3$ nanorods with a diameter of 20–30 nm, length of 70–80 nm, were anchored on the nitrogen-doped graphene sheets. After microwave treatment, the hybrids exhibit a high reversible capacity of 1016 mAh g$^{-1}$ at 0.1 A g$^{-1}$. To further improve cycling stability and capacity retention at high current density, an ultrathin $Al_2O_3$ film was deposited on electrodes via ALD. Increased capacities of 508 mAh g$^{-1}$ at 2 A g$^{-1}$ for 200 cycles and 249 mAh g$^{-1}$ for 2000 cycles at 20 A g$^{-1}$ can be achieved due to the enhanced stability of ALD coated anodes. The rational design of synergizing porous active materials, highly conductive 2D nanosheets and ultrathin alumina coating shows a great promise as advanced electrodes with excellent electrochemical performance for ultrafast and super-long life time for high-performance and high-power LIBs.

## Acknowledgements

REFERENCES

[1] Tarascon J, Armand M. Issues and challenges facing rechargeable lithium batteries. Nature 2001;414:359–67.
[2] Taberna P, Mitra S, Poizot P, Simon P, Tarascon J. High rate capabilities $Fe_3O_4$-based Cu nano-architectured electrodes for lithium-ion battery applications. Nat Mater 2006;5:567–73.
[3] Scrosati B, Garche J. Lithium batteries: status, prospects and future. J Power Sources 2010;195(9):2419–30.
[4] Kaskhedikar N, Maier J. Lithium storage in carbon nanostructures. Adv Mater 2009;21(25–26):2664–80.
[5] Poizot P, Laruelle S, Grugeon S, Dupont L, Tarascon J. Nano-sized transition-metal oxides as negative-electrode materials for lithium-ion batteries. Nature 2000;407:496–9.
[6] Armand M, Tarascon J. Building better batteries. Nature 2008;451:652–7.
[7] Park MS, Ma SB, Lee DJ, Im D, Doo SG, Yamamoto O. A highly reversible lithium metal anode. Sci Rep 2014;4. 3815-1-8.
[8] Aurbach D, Zinigrad E, Teller H, Dan P. Factors which limit the cycle life of rechargeable lithium (metal) batteries. J Electrochem Soc 2000;147(4):1274–9.
[9] Zhou X, Wan L, Guo Y. Binding $SnO_2$ nanocrystals in nitrogen-doped graphene sheets as anode materials for lithium-ion batteries. Adv Mater 2013;25(15):2152–7.
[10] Peng C, Chen B, Qin Y, Yang S, Li C, Zuo Y, et al. Facile ultrasonic synthesis of CoO quantum dot/graphene nanosheet composites with high lithium storage capacity. ACS Nano 2012;6(2):1074–81.
[11] Li Y, Tan B, Wu Y. Mesoporous $Co_3O_4$ nanowire arrays for lithium ion batteries with high capacity and rate capability. Nano Lett 2008;8(1):265–70.
[12] Reddy A, Shaijumon M, Gowda S, Ajayan P. Coaxial $MnO_2$/carbon nanotube array electrodes for high-performance lithium batteries. Nano Lett 2009;9(3):1002–6.
[13] Chen J, Xu L, Li W, Gou X. α-$Fe_2O_3$ nanotubes in gas sensor and lithium-ion battery applications. Adv Mater 2005;17(5):582–6.
[14] Zhou G, Wang D, Hou P, Li W, Li N, Liu C, et al. A nanosized $Fe_2O_3$ decorated single-walled carbon nanotube membrane as a high-performance flexible anode for lithium ion batteries. J Mater Chem 2012;22:17942–6.
[15] Liu J, Xia H, Xue D, Lu L. Double-shelled nanocapsules of $V_2O_5$-based composites as high-performance anode and cathode materials for Li ion batteries. J Am Chem Soc 2009;131(34):12086–7.

[16] Liu H, Wang G, Liu J, Qiao S, Ahn H. Highly ordered mesoporous NiO anode material for lithium ion batteries with an excellent electrochemical performance. J Mater Chem 2011;21:3046–52.

[17] Gao X, Bao J, Pan G, Zhu H, Huang P, Wu F, et al. Preparation and electrochemical performance of polycrystalline and single crystalline CuO nanorods as anode materials for Li ion battery. J Phys Chem B 2004;108(18):5547–51.

[18] Amine K, Yasuda H, Yamachi M. β-FeOOH, a new positive electrode material for lithium secondary batteries. J Power Sources 1999;81–82:221–3.

[19] Fu Y, Wang R, Xu J, Chen J, Yan Y, Narlikar A, et al. Synthesis of large arrays of aligned α-Fe$_2$O$_3$ nanowires. Chem. Phys. Lett. 2003;379(3–4):373–9.

[20] Chen J, Zhu T, Yang X, Yang H, Lou X. Top-down fabrication of α-Fe$_2$O$_3$ single-crystal nanodiscs and microparticles with tunable porosity for largely improved lithium storage properties. J Am Chem Soc 2010;132(38):13162–4.

[21] Wu C, Yin P, Zhu X, OuYang C, Xie Y. Synthesis of hematite (γ-Fe$_2$O$_3$) nanorods: diameter-size and shape effects on their applications in magnetism, lithium ion battery, and gas sensors. J Phys Chem B 2006;110(36):17806–12.

[22] Xiao Z, Xia Y, Ren Z, Liu Z, Xu G, Chao C, et al. Facile synthesis of single-crystalline mesoporous α-Fe$_2$O$_3$ and Fe$_3$O$_4$ nanorods as anode materials for lithium-ion batteries. J Mater Chem 2012;22:20566–73.

[23] Liu H, Wang G, Wang J, Wexler D. Magnetite/carbon core-shell nanorods as anode materials for lithium-ion batteries. Electrochem Commun 2008;10(12):1879–82.

[24] Luo Y, Luo J, Jiang J, Zhou W, Yang H, Qi X, et al. Seed-assisted synthesis of highly ordered TiO$_2$@α-Fe$_2$O$_3$ core/shell arrays on carbon textiles for lithium-ion battery applications. Energy Environ Sci 2012;5(4):6559–66.

[25] Zhang L, Wu H, Madhavi S, Hng H, Lou X. Formation of Fe$_2$O$_3$ microboxes with hierarchical shell structures from metal-organic frameworks and their lithium storage properties. J Am Chem Soc 2012;134(42):17388–91.

[26] Hu T, Sun X, Sun H, Yu M, Lu F, Liu C, et al. Flexible free-standing graphene-TiO$_2$ hybrid paper for use as lithium ion battery anode materials. Carbon 2013;51:322–6.

[27] Wu Z, Ren W, Xu L, Li F, Cheng H. Doped graphene sheets as anode materials with superhigh rate and large capacity for lithium ion batteries. ACS Nano 2011;5(7):5463–71.

[28] Hu T, Sun X, Sun H, Xin G, Shao D, Liu C, et al. Rapid synthesis of nitrogen-doped graphene for a lithium ion battery anode with excellent rate performance and super-long cyclic stability. Phys Chem Chem Phys 2013;16(3):1060–6.

[29] Du M, Xu C, Sun J, Gao L. One step synthesis of Fe$_2$O$_3$/nitrogen-doped graphene composite as anode materials for lithium ion batteries. Electrochim Acta 2012;80:302–7.

[30] Sun L, Wang L, Tian C, Tan T, Xie Y, Shi K, et al. Nitrogen-doped graphene with high nitrogen level via a one-step hydrothermal reaction of graphene oxide with urea for superior capacitive energy storage. RSC Adv 2012;2(10):4498–506.

[31] Kang E, Jung Y, Cavanagh A, Kim G, George S, Dillon A, et al. Fe$_3$O$_4$ nanoparticles confined in mesocellular carbon foam for high performance anode materials for lithium-ion batteries. Adv Funct Mater 2011;21(13):2430–8.

[32] Jung Y, Cavanagh A, Riley L, Kang S, Dillon A, Groner M, et al. Ultrathin direct atomic layer deposition on composite electrodes for highly durable and safe Li-ion batteries. Adv Mater 2010;22(19):2172–6.

[33] Elam J, Groner M, George S. Viscous flow reactor with quartz crystal microbalance for thin film growth by atomic layer deposition. Rev Sci Instrum 2002;73(8):2981–7.

[34] Groner M, Fabreguette F, Elam J, George S. Low-temperature Al$_2$O$_3$ atomic layer deposition. Chem Mater 2004;16(4):639–45.

[35] Ott A, Klaus J, Johnson J, George S. Al$_2$O$_3$ thin film growth on Si(100) using binary reaction sequence chemistry. Thin Solid Films 1997;292(1–2):135–44.

[36] Kamiy K, Hashimoto K, Nakanishi S. Instantaneous one-pot synthesis of Fe-N-modified graphene as an efficient electrocatalyst for the oxygen reduction reaction in acidic solutions. Chem Commun 2012;48(82):10213–5.

[37] He F, Fan J, Ma D, Zhang L, Leung C, Chan H. The attachment of Fe$_3$O$_4$ nanoparticles to graphene oxide by covalent bonding. Carbon 2010;48(11):3139–44.

[38] Zou Y, Kan J, Wang Y. Fe$_2$O$_3$-graphene rice-on-sheet nanocomposite for high and fast lithium ion storage. J Phys Chem C 2011;115(42):20747–53.